

This is the accepted manuscript made available via CHORUS. The article has been published as:

Unconventional crystal-field splitting in noncentrosymmetric BaTiO₃ thin films

Yang Song, Xiaoran Liu, Fangdi Wen, M. Kareev, Ruyi Zhang, Yujuan Pei, Jiachang Bi, Padraic Shafer, Alpha T. N'Diaye, Elke Arenholz, Se Young Park, Yanwei Cao, and J. Chakhalian

Phys. Rev. Materials **4**, 024413 — Published 24 February 2020

DOI: [10.1103/PhysRevMaterials.4.024413](https://doi.org/10.1103/PhysRevMaterials.4.024413)

Unconventional crystal field splitting in non-centrosymmetric BaTiO₃ thin films

Yang Song,^{1,2} Xiaoran Liu,³ Fangdi Wen,³ M. Kareev,³ Ruyi Zhang,^{1,2} Yujuan Pei,^{1,2} Jiachang Bi,^{1,2} Padraic Shafer,⁴ Alpha T. N'Diaye,⁴ Elke Arenholz,⁴ Se Young Park,^{5,6,*} Yanwei Cao,^{1,2,†} and J. Chakhalian³

¹*Ningbo Institute of Materials Technology and Engineering,
Chinese Academy of Sciences, Ningbo, Zhejiang 315201, China*

²*Center of Materials Science and Optoelectronics Engineering,
University of Chinese Academy of Sciences, Beijing 100049, China*

³*Department of Physics and Astronomy, Rutgers University, Piscataway, New Jersey 08854, USA*

⁴*Advanced Light Source, Lawrence Berkeley National Laboratory, Berkeley, CA 94720, USA*

⁵*Center for Correlated Electron Systems, Institute for Basic Science, Seoul 08826, Korea*

⁶*Department of Physics and Astronomy, Seoul National University, Seoul 08826, Korea*

(Dated: December 17, 2019)

Understanding the crystal field splitting and orbital polarization in non-centrosymmetric systems such as ferroelectric materials is fundamentally important. In this study, taking BaTiO₃ as a representative material we investigate titanium crystal field splitting and orbital polarization in non-centrosymmetric TiO₆ octahedra with resonant X-ray linear dichroism at Ti $L_{2,3}$ -edge. The high-quality BaTiO₃ thin films were deposited on DyScO₃ (110) single crystal substrates in a layer-by-layer way by pulsed laser deposition. The reflection high-energy electron diffraction and element specific X-ray absorption spectroscopy were performed to characterize the structural and electronic properties of the films. In sharp contrast to conventional crystal field splitting and orbital configuration ($d_{xz}/d_{yz} < d_{xy} < d_{3z^2-r^2} < d_{x^2-y^2}$ or $d_{xy} < d_{xz}/d_{yz} < d_{x^2-y^2} < d_{3z^2-r^2}$) expected from compressive or tensile epitaxial strain, respectively, it is revealed that d_{xz} , d_{yz} , and d_{xy} orbitals are nearly degenerate, whereas $d_{3z^2-r^2}$ and $d_{x^2-y^2}$ orbitals are split with an energy gap ~ 100 meV in the epitaxial BaTiO₃ films. We find that the unexpected degenerate orbitals $d_{xz}/d_{yz}/d_{xy}$ result from the competition between the orbital splitting induced by epitaxial strain and that induced by polar distortions of BaTiO₃ films. Our results provide a route to manipulate orbital degree of freedom by switching electric polarization in ferroelectric materials.

I. INTRODUCTION

Ferroelectric materials (oxide films in particular) exhibiting robust spontaneous electric polarization that can be reoriented with an external electric field, have attracted increasing attention, due to their extensive applications such as transistors, memories, and high frequency devices realized in various systems¹⁻¹⁰. For conventional ferroelectrics, the polarization emerges from a inversion-symmetry breaking lattice distortion. In BaTiO₃ (BTO), for example, the displacement of the Ti⁴⁺ cation from the center of surrounding O₆ octahedral cage gives major contribution to the induced polarization. The underlying mechanism that drives the off-centering of Ti⁴⁺ cation is attributed to pseudo Jahn-Teller effect (PJTE)¹¹⁻¹³ in which a symmetry-lowering distortion can lower the energy of system by mixing the ground state and excited states by vibronic coupling ($\partial H/\partial Q$, Q : normal displacements). The off-centering of Ti⁴⁺ cation is a typical PJTE case (usually identified in literatures as a d^0 -ness¹⁴) when the mixing of empty Ti $3d$ with filled O $2p$ orbitals results in a host of electronic configurations allowing to decrease the total energy by the distortion induced change in

the bonding between Ti $3d$ and O $2p$ orbitals¹⁵⁻¹⁸. Studies of modified crystal fields by inversion-symmetry breaking distortions and associated orbital splitting are fundamentally important for understanding the properties of ferroelectric materials and non-centrosymmetric superconductors (*e.g.*, the coexistence of superconducting and ferroelectric states in doped perovskite oxides^{19,20}). However, crystal field splittings in these systems have not been extensively studied yet^{21,22}.

To address the above concern, we take BTO thin films as a representative material to investigate crystal field splitting and orbital polarization in the presence of polar distortions induced by ordering of ferroelectric dipoles. Bulk BaTi⁴⁺O₃ with $3d^0$ electron configuration undergoes complex structural and ferroelectric phase transitions upon cooling, *e.g.*, from high temperature cubic to tetragonal (393 K), tetragonal to orthorhombic (278 K), and orthorhombic to rhombohedral (183 K), where ferroelectric properties are present below 393 K²³⁻²⁵. Moreover, under biaxial compressive strain (such as epitaxial tetragonal BTO films on DyScO₃ substrates) the transition temperature can be enhanced to nearly 500 K and the remnant polarization is at least 2.5 times higher than bulk BTO single crystals²⁶. Due to strong B -site ferroelec-

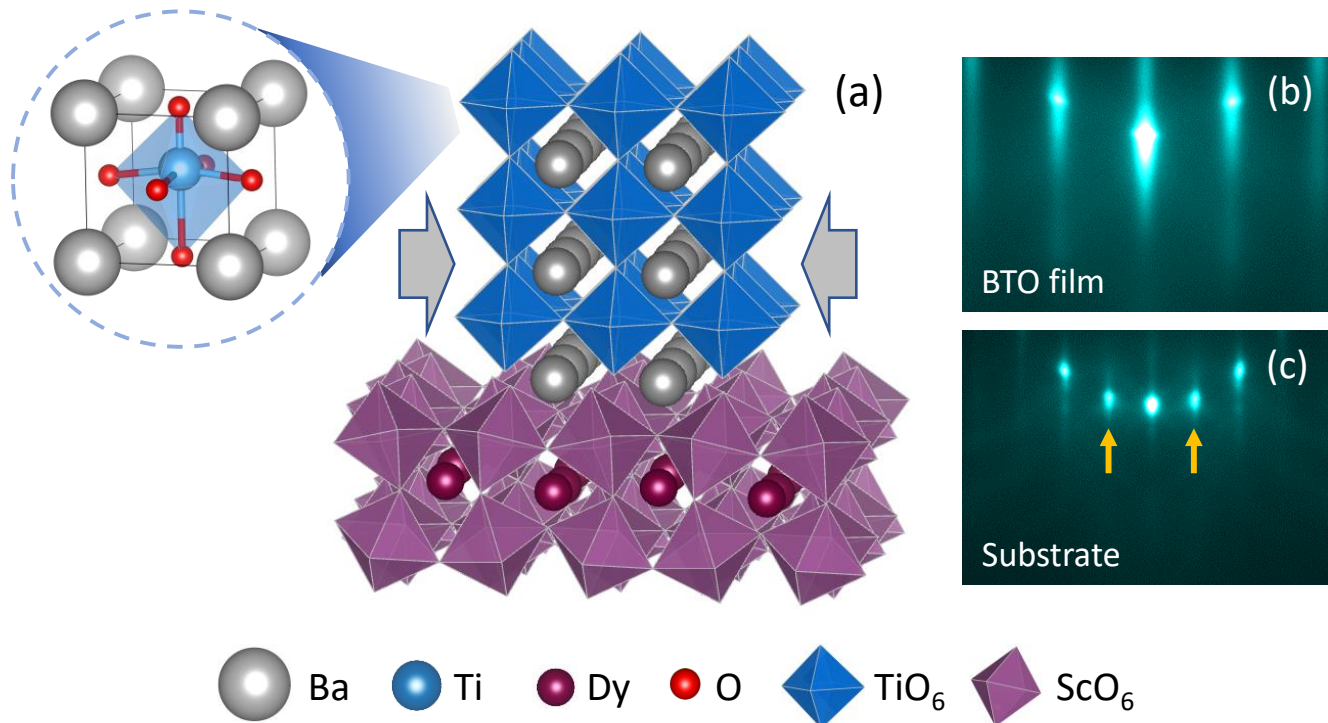


FIG. 1. (a) Schematic of epitaxial BTO film on a DSO substrate. The two arrows indicate biaxial compressive strain on BTO film. (b-c) RHEED patterns of (b) BTO film (after growth at room temperature) and (c) DSO (110) substrate (before growth). The yellow arrows indicate the half-order Bragg peaks.

tricity at room temperature^{27–31}, the BTO single crystals are widely used as ferroelectric substrates for epitaxial thin film synthesis^{32–34}, where its epitaxial films can be employed to manipulate interfacial electric field for controlling order parameters and achieving novel functionalities^{35,36}.

In this work, high-quality BTO thin films were grown on DyScO₃ (DSO) (110) single crystal substrates in a layer-by-layer way by pulsed laser deposition (PLD). The structural and electronic properties were characterized by reflection high-energy electron diffraction (RHEED) and element-specific X-ray absorption spectroscopy (XAS). In sharp contrast to conventional crystal field splitting expected with the compressive strain from DSO substrate, an anomalous orbital structure, nearly degenerate t_{2g} ($d_{xz}/d_{yz}/d_{xy}$) and split e_g ($d_{3z^2-r^2} < d_{x^2-y^2}$ about 100 meV) orbitals, was revealed in the epitaxial BTO films resulting from the competition between orbital splitting induced by compressive strain and that by spontaneous polar distortion from PJTE resulting in non-centrosymmetric TiO₆ octahedra of polar BTO films.

II. EXPERIMENTS AND FIRST-PRINCIPLES CALCULATIONS

As shown in Fig. 1, the BTO films (20 unit cells, ~ 8.2 nm) had been grown along [110] (orthorhombic notation, corresponding to [001] orientation in a pseudo-cubic notation) DSO substrates ($5 \times 5 \times 0.5$ mm³) by PLD, using a KrF excimer laser operating at $\lambda = 248$ nm and 2 Hz pulse rate with 2 J/cm² fluence. The BTO films were epitaxially grown on DSO substrates with pseudo-cubic in-plane lattice constants of $a = 3.946$ Å and $b = 3.952$ Å with 0.15% difference. During the growth, the oxygen pressure was kept at $\sim 10^{-6}$ Torr, the temperature of the substrates was ~ 850 °C (from reader of infrared pyrometers). At room temperature, the bulk lattice parameters are $a = 3.99$ Å and $c = 4.04$ Å for tetragonal BTO, and $a = 3.95$ Å for DSO (pseudo cubic). Due to the lattice mismatch, the epitaxial BTO films on DSO are under biaxial compressive strain, indicated by a pair of arrows in Fig. 1(a). In order to monitor the growth of the BTO thin film, an *in-situ* RHEED was performed during the deposition. The sharp RHEED patterns, Fig. 1(b) and (c), suggest a high-quality two-dimensional growth of the BTO films. In order to investigate the electronic structure of BTO films, lin-

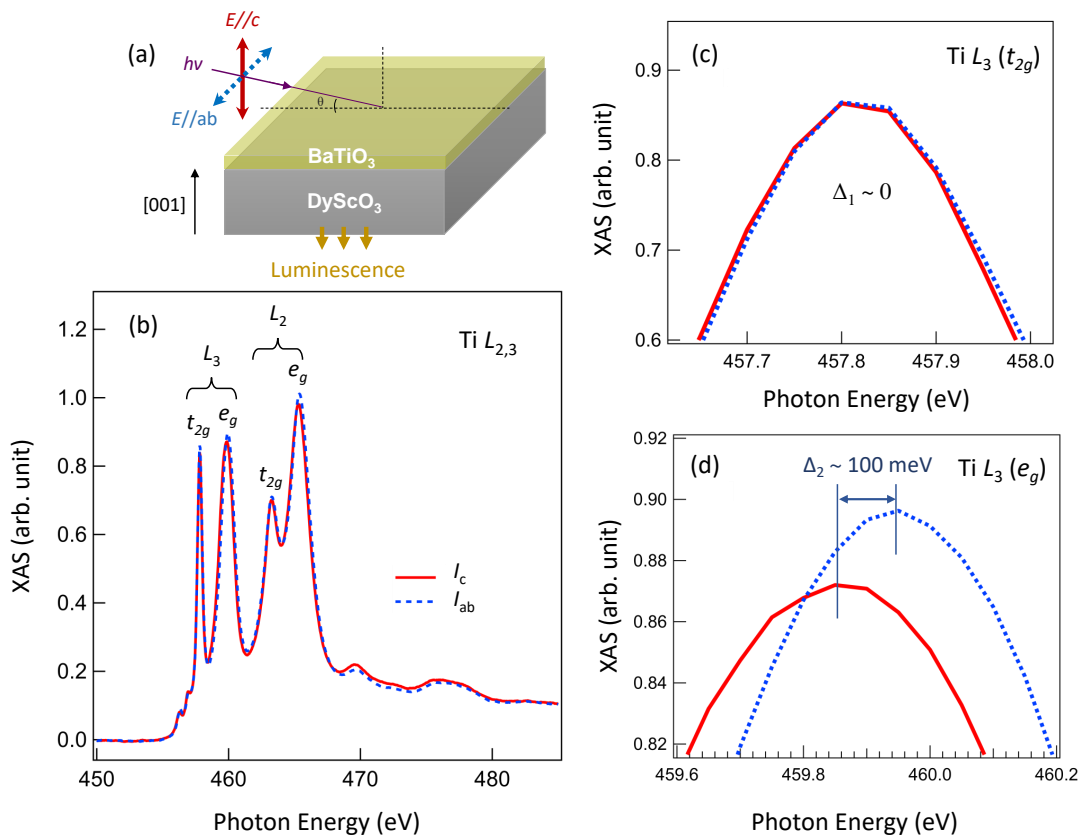


FIG. 2. (a) Schematic of experimental setup. $E \parallel c$ and $E \parallel ab$ (E is the polarization vector of the photon) indicate out-of-plane (red solid line, I_c) and in-plane (blue dash line, I_{ab}) linearly polarized incident X-ray, respectively. The grazing angle $\theta = 20^\circ$. The yellow arrows at the bottom of DSO substrate indicates the bulk-sensitive luminescence yield detection mode. The arrow along $[001]$ direction (pseudo-cubic notation) indicates the growth direction of BTO films. (b) XAS of BTO films at Ti $L_{2,3}$ -edge at room temperature. All collected spectra are repetitively measured more than six times. Enlarged XAS spectra at (c) Ti L_3 (t_{2g}) and (d) Ti L_3 (e_g) absorption peaks. Δ_1 and Δ_2 are defined as the splitting between d_{xy} and d_{xz}/d_{yz} orbitals, and between $d_{x^2-y^2}$ and $d_{3z^2-r^2}$ orbitals, respectively

early polarized XAS in luminescence yield detection mode (bulk-sensitive, see Fig. 2(a)) was performed at room temperature at beamline 4.0.2 of the Advanced Light Source (ALS, Lawrence Berkeley National Laboratory)³⁷, and the preliminary data were collected at beamline 6.3.1. We have carried out first-principles density-functional theory (DFT) calculations within the local density approximation (LDA)^{38,39}. The calculations were performed using the Vienna *ab-initio* simulation package (VASP)^{40,41}. The projector augmented wave (PAW)⁴² was used with an energy cut-off of 600 eV. The Brillouin zone was sampled with a $8 \times 8 \times 8$ k -point grid for 5-atom unit cell of BTO. Convergence is reached if the consecutive energy difference is less than 10^{-6} eV for electronic iterations and 10^{-5} eV for ionic relaxations. The polarization was calculated using the Berry-phase method⁴³ as implemented in VASP. The tight-binding parameters for Ti d orbitals were calculated by Wannier90 package⁴⁴. For strained

bulk calculation, we have used a tetragonal in-plane unit cell ($a = b$), due to the small difference in the a and b lattice constants (0.15 %) having negligible effects on projected density of states (see Appendix A for details). The simulated XAS spectra at Ti $L_{2,3}$ -edge were performed using the CTM4XAS code. In calculation, the electron interactions were taken into account by means of the Slater integrals F_{dd} , F_{pd} , and G_{pd} , which were scaled down to 80 % of their *ab initio* values^{45,46}.

III. RESULTS AND DISCUSSIONS

Figure 2(b) shows the XAS spectra of BTO films at Ti $L_{2,3}$ -edge. There are four well split characteristic peaks, arising from the excitation from Ti $2p$ to Ti $3d$ states (the electronic configuration changes from Ti $2p^6 3d^0$ to $2p^5 3d^1$). Generally, in octahedral symmetry, the transition-metal d bands split into t_{2g} (d_{xy} , d_{xz} , d_{yz}) and e_g ($d_{3z^2-r^2}$, $d_{x^2-y^2}$)⁴⁷⁻⁵³. The

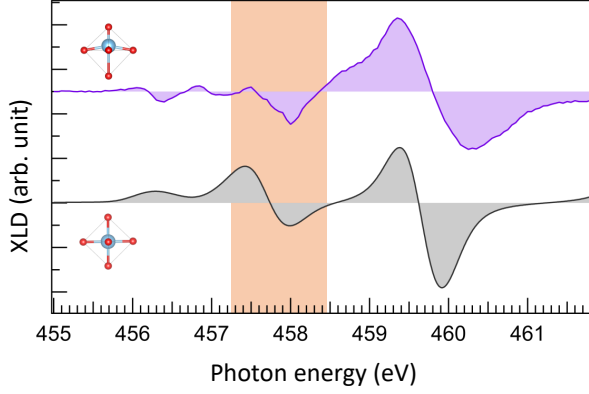


FIG. 3. XLD of BTO thin film (upper panel) measured at room temperature with out-of-plane polar distortion. Simulated XLD of tetragonal BTO (lower panel) without polar distortion. The rectangular orange shadow highlights the nearly degenerate t_{2g} orbitals which is in contrast to the clear sign change observed in t_{2g} orbitals of non-polar BTO.

degenerate t_{2g} and e_g bands further split when the octahedron experiences uniaxial elongation or compression along the c -axis⁵⁴, leading to the orbital structure of $d_{xz}/d_{yz} < d_{xy} < d_{3z^2-r^2} < d_{x^2-y^2}$ or $d_{xy} < d_{xz}/d_{yz} < d_{x^2-y^2} < d_{3z^2-r^2}$, respectively. Using that intensity of linearly polarized XAS carries the information of crystal field splitting and orbital polarization⁴⁷⁻⁵³, Figure 2(c) and (d) show the differences between out-of-plane (I_c) and in-plane (I_{ab}) polarized XAS. As seen, the t_{2g} orbitals are nearly degenerate ($\Delta_1 \sim 0$, see Fig. 2(c)), whereas the splitting Δ_2 between $d_{x^2-y^2}$ and $d_{3z^2-r^2}$ orbitals in e_g state is about 100 meV, shown in Fig. 2(d). The same orbital splitting is observed at Ti L_{2-3} edge as well. This kind of orbital structure in BTO films ($d_{xz}/d_{yz}/d_{xy} < d_{3z^2-r^2} < d_{x^2-y^2}$) is unexpected and in sharp contrast to conventional crystal field splitting ($d_{xz}/d_{yz} < d_{xy} < d_{3z^2-r^2} < d_{x^2-y^2}$) in elongated TiO_6 octahedra along the c -axis⁵⁵.

To further understand this anomalous orbital structure in the BTO films, we obtain the spectra of X-ray linear dichroism (XLD), which is defined as $\text{XLD} = I_c - I_{ab}$ in this work. Fig. 3 shows the XLD spectra of the strained BTO with out-of-plane polar distortion at room temperature at Ti $L_{2,3}$ edge and the XLD spectra of tetragonal BTO without polar distortion simulated by atomic multiplet scattering calculations using CTM4MAX code⁵⁶. As highlighted area in Fig. 3, the XLD of the BTO films shows nearly degenerate ($d_{xz} \simeq d_{yz} \simeq d_{xy}$) t_{2g} orbitals, whereas e_g orbitals show clear dichroism with $d_{3z^2-r^2} < d_{x^2-y^2}$.

The discrepancy between the degenerate t_{2g} orbitals and the expected crystal field splitting from the compressive strain

strongly suggest an additional mechanism behind unusual orbital splitting. Since the bulk BTO is ferroelectric at room temperature²³, it is natural to include the polar distortion in BTO and investigate its contribution to the orbital splitting. From epitaxial growth, the BTO thin film is under a compressive strain about 1.25% relative to the cubic phase (4.00 Å). This leads to the orbital splitting having d_{xz}/d_{yz} orbitals lower than d_{xy} ³⁷. Using the first-principles DFT method, we first calculate the effect of epitaxial strain on orbital splitting from the change in the c/a ratio without considering the polar distortion. With 1.25% compressive strain based on the lattice mismatch between BTO and DSO, the c/a ratio obtained by strained-bulk calculation increases to 1.02. Next, we allow a polarization along the c -axis, experimentally observed under the compressive strain^{57,58}. The relaxed atomic structure with 1.25% compressive epitaxial strain lowers the total energy by 19 meV per formula unit from a polar distortion, mainly contributed by Ti displacement from the center of the octahedron with Ti-O-Ti angle of 172° . The calculated polarization is $33 \mu\text{C}/\text{cm}^2$ along the c -axis with further increase in the c/a ratio to 1.04.

In order to investigate the effect of the strain and polar distortion to orbital polarization, we consider two atomic configurations: one with compressive strain with $c/a = 1.04$ with zero polar distortion and the other with cubic lattice constant with 1.25% compressive strain applied for all three lattice constants and with the polar distortion of the strained bulk calculation. The projected density of states (PDOS) and Wannier tight-binding parameters are presented in Fig. 4 and Table I, respectively. In Fig. 4(a), we find that the effect of the compressive strain is straightforwardly shown in the PDOS with $d_{xz}/d_{yz} < d_{xy}$ and $d_{3z^2-r^2} < d_{x^2-y^2}$ orbital splitting, consistent with on-site energy difference $E_{xz/yz} - E_{xy} = -0.13$ eV for t_{2g} orbitals and $E_{3z^2-r^2} - E_{x^2-y^2} = -0.45$ eV for e_g orbitals (Table I). We note that the splitting between t_{2g} orbitals is smaller than that of e_g orbitals due to the relatively weaker π bonding of t_{2g} orbitals compared to the σ bonding of e_g . In contrast, the inclusion of the polar distortion without strain (cubic lattice constants) results in the opposite trend in the PDOS as shown in Fig. 4(b): $d_{xz}/d_{yz} > d_{xy}$ and $d_{3z^2-r^2} > d_{x^2-y^2}$ orbital splitting, consistent with the on-site energy difference of $E_{xz/yz} - E_{xy} = 0.15$ eV for t_{2g} orbitals and of $E_{3z^2-r^2} - E_{x^2-y^2} = 0.13$ eV for e_g orbitals (Table I). We note that the splitting between the t_{2g} orbitals from the polar distortion is larger than that between e_g orbitals, consistent with relatively larger reduction in the in-plane hopping $t_{xz/yz}^{\parallel}$ about 50 meV than that of $t_{x^2-y^2}^{\parallel}$ about 20 meV compared with the hopping parameters of cubic BTO. This suggests that

TABLE I. On-site energies and major hopping parameters of Ti d orbitals for BTO (in eV) obtained from Wannier functions of Ti d band. For hopping parameter t , \parallel and \perp represent the in-plane and out-of-plane hopping, respectively.

	On-site energy difference		Intra orbital hopping				
	$E_{xz/yz} - E_{xy}$	$E_{3z^2-r^2} - E_{x^2-y^2}$	t_{xy}^{\parallel}	$t_{xz/yz}^{\parallel}$	$t_{xz/yz}^{\perp}$	$t_{x^2-y^2}^{\parallel}$	$t_{3z^2-r^2}^{\perp}$
Cubic	0	0	-0.31	-0.31	-0.31	-0.50	-0.66
Tetragonal ($P = 0$)	-0.13	-0.45	-0.30	-0.33	-0.25	-0.50	-0.64
Cubic ($P \neq 0$)	0.15	0.13	-0.30	-0.26	-0.28	-0.48	-0.66

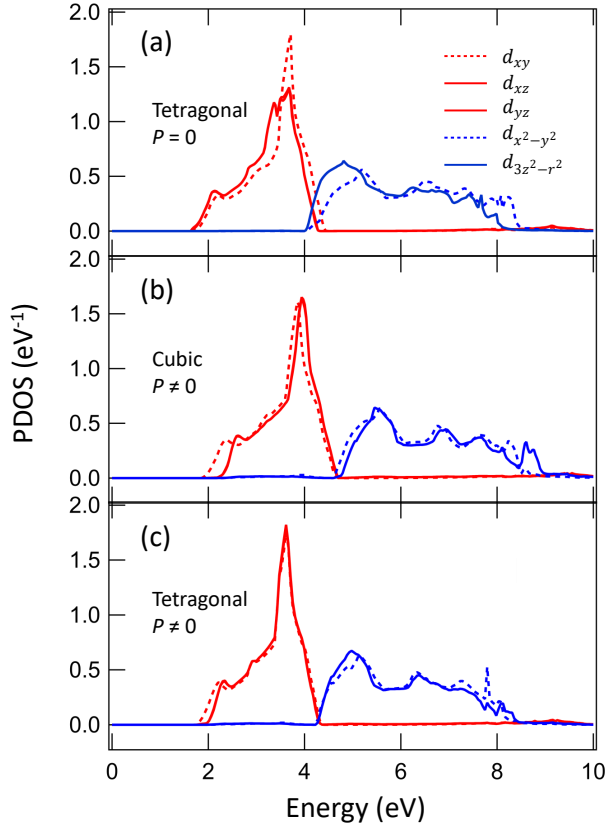


FIG. 4. PDOS of the strained bulk calculations with 1.25% biaxial compressive strain. PDOS of (a) tetragonal BTO with zero polarizations ($c/a = 1.04$), (b) cubic BTO with Ti polar distortion, and (c) fully relaxed tetragonal BTO with Ti polar distortion along c direction ($c/a = 1.01$).

the bonding between the t_{2g} orbitals is more sensitive to the Ti-O-Ti angle than that between the e_g orbitals. In the case without epitaxial constraints (fully relaxed), the spontaneous polarization in the c -direction by PJTE increases c/a ratio to 1.01 with a -lattice constant decrease about 0.35%. Due to the t_{2g} orbital splitting being more sensitive to the polar distortion than to the increased c/a ratio, we find $d_{xy} < d_{xz}/d_{yz}$ orbital splitting (Fig. 4(c)), which is consistent with transport measurement of BTO thin films⁵⁹. In contrast, we find $d_{3z^2-r^2}$

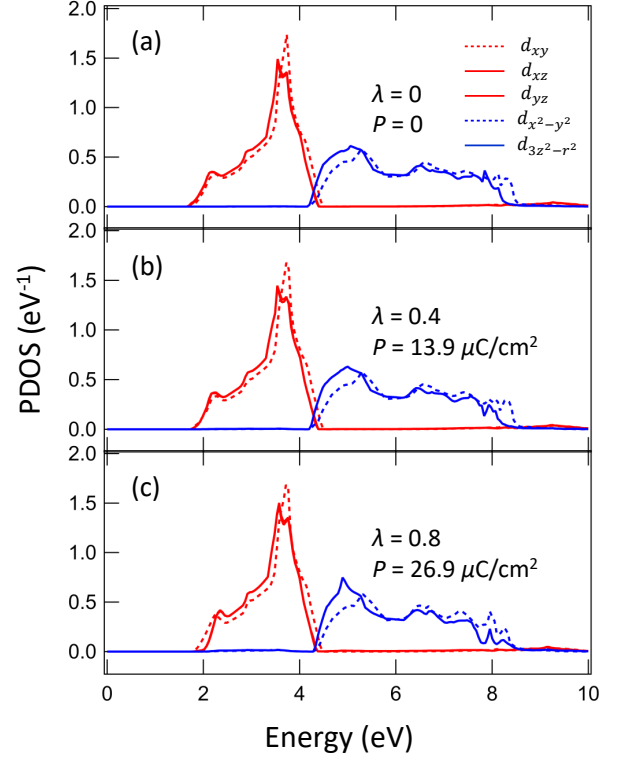


FIG. 5. PDOS of the atomic structures linearly interpolated between non-polar strained bulk BTO structure with $c/a = 1.02$ and polar strained bulk BTO structure with $P = 33 \mu\text{C}/\text{cm}^2$. The symbol λ is defined as the parameter of the linear interpolation ($\lambda = 0$ and 1 for non-polar and polar structures). PDOS for (a) $\lambda = 0$, (b) $\lambda = 0.4$ ($P = 14 \mu\text{C}/\text{cm}^2$) and (c) $\lambda = 0.8$ ($P = 27 \mu\text{C}/\text{cm}^2$).

$< d_{x^2-y^2}$, due to the e_g orbital being more sensitive to the increased c/a ratio than to the polar distortion.

The degeneracy of the t_{2g} orbitals observed in XLD can be understood by combined effects from the compressive strain and from polar distortion. The degeneracy of the t_{2g} orbitals is induced by the cancellation between orbital splitting from the compressive strain and polar distortion which are similar in amount (-0.13 eV vs 0.15 meV), while the degeneracy of e_g orbitals is lifted due to larger difference of the orbital splitting from the strain and polar distortion (-0.45 eV vs 0.13 eV). To

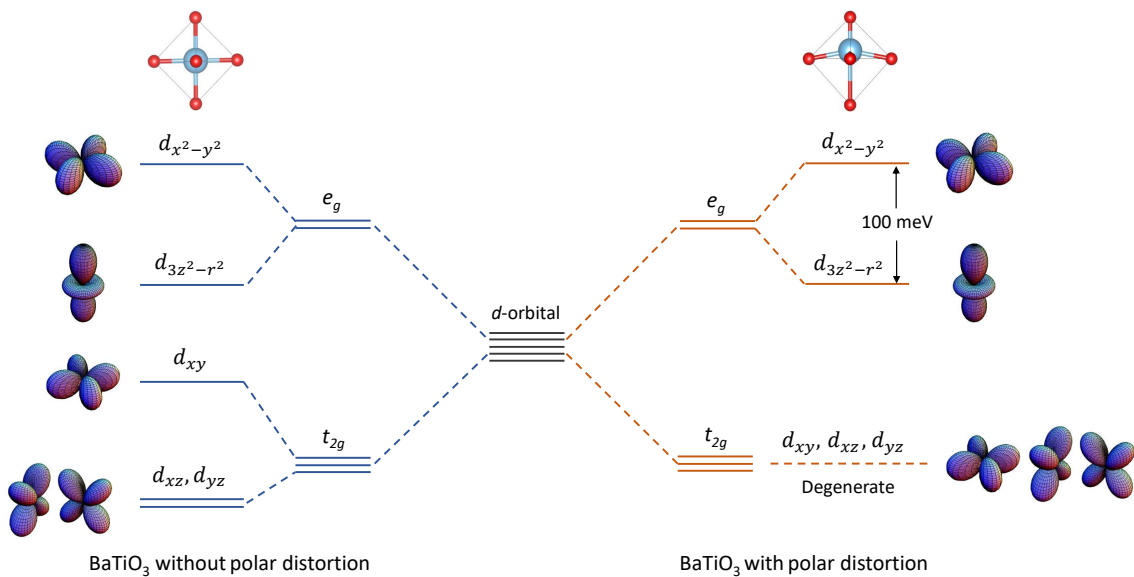


FIG. 6. Comparison of crystal-field splitting between strained BaTiO₃ (a) without and (b) with polar distortions.

confirm this idea, we calculate the PDOS of the structures obtained by linear interpolation between the strained bulk atomic structure without polarization ($c/a = 1.02$) parameterized by $\lambda = 0$ and strained bulk atomic structure with out-of-plane polarization ($c/a = 1.04$) parameterized by $\lambda = 1$. Figure 5 shows the PDOS with $\lambda = 0, 0.4$, and 0.8 . For the all values of the λ , the splitting of the e_g orbital ($d_{3z^2-r^2} < d_{x^2-y^2}$) is maintained due to the splitting from the elongated c -axis ($c/a > 1.02$) dominating the e_g orbital splitting. In contrast, the sign change in the t_{2g} orbital splitting is clearly seen for $\lambda = 0$ and $\lambda = 0.8$. In particular, for $\lambda = 0.4$, the t_{2g} orbitals are closely degenerate while e_g orbitals split about 0.3 eV, consistent with the experimental data. For the $\lambda = 0.4$, the polarization value reduced to about 42% of the $\lambda = 1$ structure, which may come from the finite thickness of BTO, suppressing the polarization.

Here, we compare the crystal-field splitting between the strained BTO without and with the polar distortion, illustrated in Fig. 6. The unusual orbital structures we have observed in this work may provide a clue to understand the peculiar band splitting of BTO investigated by angle-resolved photoemission spectroscopy (ARPES)⁶⁰, by including the crystal field splitting from polar distortions. Our finding here provides an effective way to manipulate orbital degree of freedom by manipulating ferroelectric polarization which could be used to design exotic quantum states, such as metal-insulator transition, superconductivity, and colossal magnetoresistance.

IV. CONCLUSION

In summary, we have synthesized high-quality BTO thin films on DSO substrates with a layer-by-layer growth by PLD and characterized the structural and electronic properties by RHEED, element-specific XAS/XLD, and first-principles calculations. In sharp contrast to conventional crystal field splitting and orbital configuration ($d_{xz}/d_{yz} < d_{xy} < d_{3z^2-r^2} < d_{x^2-y^2}$) in elongated TiO₆ octahedra, the XLD spectra reveals that the orbital structure in BTO films is unconventional: nearly degenerate t_{2g} ($d_{xz}/d_{yz}/d_{xy}$) and split e_g ($d_{3z^2-r^2} < d_{x^2-y^2}$ with a gap ~ 100 meV) orbitals. The first-principles DFT calculations show that this unexpected degenerate t_{2g} orbitals are from the competition between the orbital splitting from the compressive strain and polar distortion. Our work could pave a way to design exotic quantum states (such as tunable multiferroic properties) by manipulating the orbital degree of freedom using the switchable ferroelectric polarizations.

ACKNOWLEDGMENTS

We acknowledge insightful discussions with Darren C. Peets. This work is supported by the National Natural Science Foundation of China (Grant No. 11874058), the Pioneer Hundred Talents Program of the Chinese Academy of Sciences, Ningbo 3315 Innovation Team, and the Ningbo Science and Technology Bureau (Grant No. 2018B10060). J.

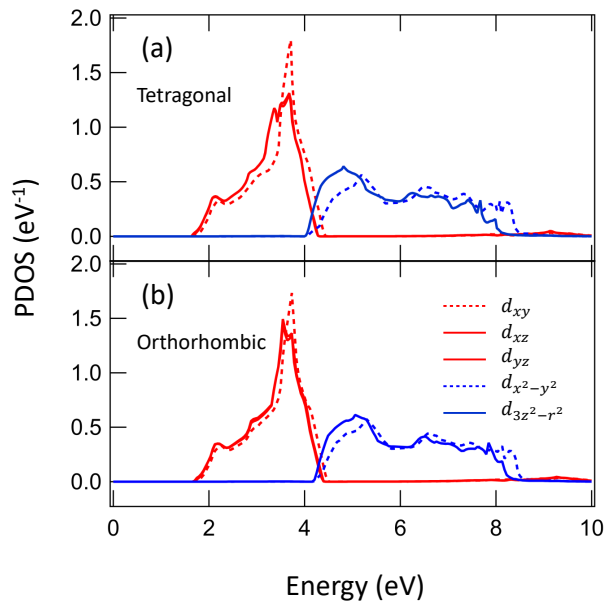


FIG. A.1. PDOS of (a) tetragonal ($a = 3.9005 \text{ \AA}$) and (b) orthorhombic ($a = 3.9034 \text{ \AA}$, $b = 3.8976 \text{ \AA}$) BTO, both with $P = 0$.

C. acknowledges support from the Gordon and Betty Moore Foundation EPiQS Initiative through Grant No. GBMF4534. This research used resources of the Advanced Light Source, which is a DOE Office of Science User Facility under contract No. DE-AC02-05CH11231. S. P. acknowledges support from the Institute for Basic Science in Korea (Grant No. IBS-R009-D1).

Appendix A

Fig. A1 shows calculated PDOS of tetragonal ($a = 3.9005 \text{ \AA}$, $c = 3.9856 \text{ \AA}$) and orthorhombic ($a = 3.9034 \text{ \AA}$, $b = 3.8976 \text{ \AA}$, $c = 3.9856 \text{ \AA}$) BTO with strained a (+0.76 %) and b (-0.76 %) lattice constants relative to the tetragonal structure. The PDOS shows almost identical PDOS between the two structures due to the small difference in the in-plane lattice constants.

* sp2829@snu.ac.kr

† ywcao@nimte.ac.cn

¹ L. W. Martin and A. M. Rappe, Nat. Rev. Mater. **2**, 16087 (2016).

² R. Resta, Rev. Mod. Phys. **66**, 899 (1994).

³ M. Dawber, K. M. Rabe, and J. F. Scott, Rev. Mod. Phys. **77**, 1083 (2005).

⁴ D. G. Schlom, L. Q. Chen, C. B. Eom, K. M. Rabe, S. K. Streiffer, and J. M. Triscone, Annu. Rev. Mater. Res. **37**, 589 (2007).

⁵ N. Setter, D. Damjanovic, L. Eng, G. Fox, S. Gevorgian, S. Hong, A. Kingon, H. Kohlstedt, N. Y. Park, G. B. Stephenson, I. Stolitchnov, A. K. Taganstev, D. V. Taylor, T. Yamada, and S. Streiffer, J. Appl. Phys. **100**, 051606 (2006).

⁶ R. Ramesh and N. A. Spaldin, Nat. Mater. **6**, 21 (2007).

⁷ W. Eerenstein, N. D. Mathur, and J. F. Scott, Nature **442**, 759 (2006).

⁸ R. E. Cohen, Nature **358**, 136 (1992).

⁹ N. A. Spaldin and M. Fiebig, Science **309**, 391 (2005).

¹⁰ W. Yun, J. Urban, Q. Gu, and H. Park, Nano Lett. **2**, 447 (2002).

¹¹ I. B. Bersuker, Chem. Rev. **113**, 1351-1390, (2013).

¹² I. Bersuker, Physics Letters **20**, 589-590, (1966)

¹³ V. Polinger, P. Garcia-Fernandez, and I. Bersuker, Physica B: Condensed Matter **457**, 296-309, (2015).

¹⁴ N. A. Hill, J. Phys. Chem. B **104**, 6694-6709, (2000)

¹⁵ H. N. Lee, H. M. Christen, M. F. Chisholm, C. M. Rouleau, and D. H. Lowndes, Nature **433**, 395 (2005).

¹⁶ H. Guo, Z. Wang, S. Dong, S. Ghosh, M. Saghayezhian, L. Chen, Y. Weng, A. Herklotz, T. Z. Ward, R. Jin, S. T. Pantelides, Y. Zhu, J. Zhang, and E. W. Plummer, Proc. Natl. Acad. Sci. U.S.A. **114**,

E5062 (2017).

¹⁷ Y. Cao, Z. Wang, S. Y. Park, Y. Yuan, X. Liu, S. M. Nikitin, H. Akamatsu, M. Kareev, S. Middey, D. Meyers, P. Thompson, P.J. Ryan, P. Shafer, A. NDiaye, E. Arenholz, V. Gopalan, Y. Zhu, K. M. Rabe, and J. Chakhalian, Nat. Commun. **9**, 1547 (2018).

¹⁸ F. Cordero, F. Trequattrini, F. Craciun, H. Langhammer, D. Quiroga, and P. Silva Jr. Phys. Rev. B **99**, 064106 (2019).

¹⁹ M. Gabay and J.-M. Triscone, Nat. Phys. **13**, 624, (2017).

²⁰ C. W. Rischau, X. Lin, C. P. Grams, D. Finck, S. Harms, J. Engelmayr, T. Lorenz, Y. Gallais, B. Fauqu, J. Hemberger, and K. Behnia, Nat. Phys. **13**, 643, (2017).

²¹ C. Schmitz-Antoniak, D. Schmitz, P. Borisov, F. de Groot, S. Stienen, A. Warland, B. Krumme, R. Feyerherm, E. Dudzik, W. Kleemann, and H. Wende, Nat. Commun. **4**, 2051 (2013).

²² E. Arenholz, G. Van der Laan, A. Fraile-Rodriguez, P. Yu, Q. He, and R. Ramesh, Phys. Rev. B **82**, 140103 (2010).

²³ G.H. Kwei, A. C. Lawson, S. J. L. Billinge and S.-W. Cheong, J. Phys. Chem. **97** 2368 (1993)

²⁴ T. Ishidate, S. Abe, H. Takahashi, and N. Mōri, Phys. Rev. Lett. **78**, 2397 (1997).

²⁵ S. A. Hayward and E. K. H. Salje, J. Phys.: Condens. Matter **14**, L599 (2002).

²⁶ K. Choi, M. Biegalski, Y. Li, A. Sharan, J. Schubert, R. Uecker, P. Reiche, Y. Chen, X. Pan, V. Gopalan, L. Chen, D. Schlom, and C. Emo, Science **306**, 1005 (2004).

²⁷ M. B. Smith, K. Page, T. Siegrist, P. L. Redmond, E. C. Walter, R. Seshadri, L. E. Brus, and M. L. Steigerwald, J. Am. Chem. Soc. **130**, 6955 (2008).

- ²⁸ C. Ma, K. Jin, C. Ge, and G. Yang, *Phys. Rev. B* **97**, 115103 (2018).
- ²⁹ P. Blom, R. Wolf, J. Cillessen, and M. Krijn, *Phys. Rev. Lett.* **73**, 2107 (1994).
- ³⁰ A. Kholkin, E. Colla, A. Tagantsev, D. Taylor, and N. Setter, *Appl. Phys. Lett.* **68**, 2577 (1996).
- ³¹ C. Ma, X. He, and K. Jin, *Phys. Rev. B* **96**, 035140 (2017).
- ³² A. Alberca, C. Munuera, J. Tornos, F. Mompean, N. Biskup, A. Ruiz, N. Nemes, A. de Andres, C. Len, J. Santamara and M. Garca-Hernandez. *Phys. Rev. B* **86**, 144416 (2012).
- ³³ S. Brivio, D. Petti, R. Bertacco, and J. Cezar. *Appl. Phys. Lett.* **98**, 092505 (2011).
- ³⁴ M. Lee, T. Nath, C. Eom, M. Smoak, and F. Tsui. *Appl. Phys. Lett.* **77**, 3547-3549 (2000).
- ³⁵ L. Wang, Q. Feng, Y. Kim, R. Kim, K. H. Lee, S. D. Pollard, Y. J. Shin, H. Zhou, W. Peng, D. Lee, W. Meng, H. Yang, J. H. Han, M. Kim, Q. Lu, and T. W. Noh. *Nat. Mater.* **17**, 1087, (2018).
- ³⁶ B. Cui, C. Song, H. Mao, Y. Yan, F. Li, S. Gao, J. Peng, F. Zeng, and F. Pan, *Adv. Funct. Mater.* **26**, 753 (2016).
- ³⁷ Y. Cao, P. Shafer, X. Liu, D. Meyers, M. Kareev, S. Middey, J. Freeland, E. Arenholz, and J. Chakhalian. *Appl. Phys. Lett.* **107**, 112401 (2015).
- ³⁸ D. M. Ceperley and B. J. Alder, *Phys. Rev. Lett.* **45**, 566 (1980).
- ³⁹ J. P. Perdew and A. Zunger, *Phys. Rev. B* **23**, 5048 (1981).
- ⁴⁰ G. Kresse and J. Furthmüller, *Phys. Rev. B* **54**, 11169 (1996).
- ⁴¹ G. Kresse, and D. Joubert, *Phys. Rev. B* **59**, 1758 (1999).
- ⁴² P. E. Blöchl, *Phys. Rev. B* **50**, 17953 (1994).
- ⁴³ R. D. King-Smith and D. Vanderbilt, *Phys. Rev. B* **47**, 1651 (1993).
- ⁴⁴ A. A. Mostofi, J. R. Yates, G. Pizzi, Y.-S. Lee, I. Souza, D. Vanderbilt, and N. Marzari, *Comp. Phys. Commun.* **185**, 2309 (2014).
- ⁴⁵ E. Stavitski and F. M. De Groot, *Micron* **41**, 687694 (2010).
- ⁴⁶ F. M. F. de Groot, J. C. Fuggle, B. T. Thole, and G. A. Sawatzky, *Phys. Rev. B* **41**, 928937 (1990).
- ⁴⁷ J. S. Lee, Y. W. Xie, H. K. Sato, C. Bell, Y. Hikita, H. Y. Hwang, and C. C. Kao, *Nat. Mater.* **12**, 703 (2013).
- ⁴⁸ M. Salluzzo, J. C. Cezar, N. B. Brookes, V. Bisogni, G. M. De Luca, C. Richter, S. Thiel, J. Mannhart, M. Huijben, A. Brinkman, G. Rijnders, and G. Ghiringhelli, *Phys. Rev. Lett.* **102**, 166804 (2009).
- ⁴⁹ M. Salluzzo, S. Gariglio, D. Stornaiuolo, V. Sessi, S. Rusponi, C. Piamonteze, G. M. De Luca, M. Minola, D. Marré, A. Gadaleta, H. Brune, F. Nolting, N. B. Brookes, and G. Ghiringhelli, *Phys. Rev. Lett.* **111**, 087204 (2013).
- ⁵⁰ M. Salluzzo, S. Gariglio, X. Torrelles, Z. Ristic, R. Di Capua, J. Drnec, M. Moretti Sala, G. Ghiringhelli, R. Felici, and N. B. Brookes, *Adv. Mater.* **25**, 2333 (2013).
- ⁵¹ D. Pesquera, M. Scigaj, P. Gargiani, A. Barla, J. Herrero-Martín, E. Pellegrin, S. M. Valvidares, J. Gázquez, M. Varela, N. Dix, J. Fontcuberta, F. Sánchez, and G. Herranz, *Phys. Rev. Lett.* **113**, 156802 (2014).
- ⁵² Y. Cao, Z. Yang, M. Kareev, X. Liu, D. Meyers, S. Middey, D. Choudhury, P. Shafer, J. Guo, J. W. Freeland, E. Arenholz, L. Gu, and J. Chakhalian, *Phys. Rev. Lett.* **116**, 076802 (2016).
- ⁵³ Y. Cao, X. Liu, P. Shafer, S. Middey, D. Meyers, M. Kareev, Z. Zhong, J.W. Kim, P. Ryan, E. Arenholz, and J. Chakhalian, *npj Quantum Mater.* **1**, 16009 (2016).
- ⁵⁴ D. Louca, T. Egami, E. Brosha, H. Rder, and A. Bishop, *Phys. Rev. B* **56**, R8475 (1997).
- ⁵⁵ Y. Cao, S. Park, X. Liu, D. Choudhury, S. Middey, D. Meyers, M. Kareev, P. Shafer, E. Arenholz, and J. Chakhalian, *Appl. Phys. Lett.* **109**, 152905 (2016).
- ⁵⁶ W. Fan, Y. Song, J. Bi, Y. Pei, R. Zhang, and Y. Cao. *AIP Advances* **9**, 065213, (2019).
- ⁵⁷ Oswaldo Dieguez, Silvia Tinte, A. Antons, Claudia Bungaro, J. B. Neaton, Karin M. Rabe, and David Vanderbilt, *Phys. Rev. B* **69**, 212101 (2004).
- ⁵⁸ C. Housecroft and A. Sharpe. *Inorganic Chemistry*, England: Pearson, 673-700, (2015).
- ⁵⁹ K. Takahashi, Y. Matsubara, M. Bahramy, N. Ogawa, D. Hashizume, Y. Tokura, and M. Kawasaki. *Sci. Rep.* **7**, 4631, (2017).
- ⁶⁰ T. Rdel, M. Vivek, F. Fortuna, P. Le Fvre, F. Bertran, R. Weht, J. Goniakowski, M. Gabay, and A. Santander-Syro. *Phys. Rev. B* **96**, 041121 (2017).